

Article

Removal of Trichloroethylene from Water by Bimetallic Ni/Fe Nanoparticles

Xiaonan Liu , Minghong Wu * and Jian Zhao

Key Laboratory of Organic Compound Pollution Control Engineering,
School of Environmental and Chemical Engineering, Shanghai University, Shanghai 200444, China;
liaoxiaonan@shu.edu.cn (X.L.); zhaojian1997@shu.edu.cn (J.Z.)

* Correspondence: mhwu@shu.edu.cn; Tel.: +86-21-6613-7508

Abstract: Chlorinated organic solvents (COSs) are a significant threat to human beings. In this study, nanoscale bimetallic Ni/Fe particles were synthesized from the reaction of sodium borohydride (NaBH_4) with the reduction of Ni^{2+} and Fe^{2+} in an aqueous solution. The synthesized nanoscale zero-valent iron (nZVI) and Ni-nZVI were characterized by SEM (scanning electron microscopy), XRD (X-ray diffractometer), Brunauer–Emmett–Teller (BET), and transmission electron microscopy (TEM). The removal performance of trichloroethylene (TCE) over the nZVI catalyst and Ni-nZVI was evaluated. Ni-nZVI with different Ni contents exhibited good reactivity towards the dechlorination of TCE over a 1h period, and the pseudo-first-order rate constant for TCE dechlorination by Ni-nZVI was 1.4–3.5 times higher than that of nZVI. Ni-nZVI with 5 wt% Ni contents exhibited the best dechlorination effect; the removal rates of TCE and its by-product dichloroethylene (DCE) were 100% and 63.69%, respectively. These results indicated that the Ni nanoparticles as the second dopant metal were better than nZVI for TCE degradation. This determination of the optimal Ni-nZVI load ratio provides a factual and theoretical basis for the subsequent application of nano-metal binding in the environment.

Keywords: zero-valent iron; nickel-zero-valent iron; trichloroethyl; dichloroethylene



Citation: Liu, X.; Wu, M.; Zhao, J. Removal of Trichloroethylene from Water by Bimetallic Ni/Fe Nanoparticles. *Water* **2022**, *14*, 1616. <https://doi.org/10.3390/w14101616>

Academic Editor: Andrea G. Capodaglio

Received: 23 March 2022

Accepted: 11 May 2022

Published: 18 May 2022

Publisher's Note: MDPI stays neutral with regard to jurisdictional claims in published maps and institutional affiliations.



Copyright: © 2022 by the authors. Licensee MDPI, Basel, Switzerland. This article is an open access article distributed under the terms and conditions of the Creative Commons Attribution (CC BY) license (<https://creativecommons.org/licenses/by/4.0/>).

1. Introduction

Chlorinated organic solvents (COSs) are the most commonly used organic solvents in the chemical industry [1]. Excessive use of COSs, non-compliance with production processes, and illegal discharge jointly lead to organic contamination and leakage, posing a significant threat to human beings [2]. In recent years, due to the development of nanomaterials, which have high reducing activity, there have been more and more studies on the remediation of groundwater and soil with nanometer zero-valent metals. Fe is not only a safe, cheap, and easily available metal, but also, as zero-valent iron, has the characteristics of high efficiency and could be used as a permeability barrier material for remediation of groundwater pollution, which has broad development prospects [3,4]. Accordingly, nano-zero-valent iron (nZVI) has been proven to be able to successfully degrade COCs, including carbon tetrachloride (CT), trichloroethylene (TCE), etc., and to achieve a good removal effect in the remediation of contaminated sites. Zero-valent iron has mainly been used as a strong electron donor, and the electrons released are reduced with oxidants such as hydrogen ions, oxygen, water, and pollutants. This results in the low electron efficiency of zero-valent iron because many of the electrons donated by ZVI are used inside reactions, such as the reduction of water to hydrogen, rather than in the reduction of target contaminants [5,6]. In addition, these monometal degradation processes might produce more toxic intermediates, such as dichloroethylene (DCM) and vinyl chloride [7].

Bimetallic nanomaterials have the advantages of higher efficiency and more complete dechlorination, making the bimetallic system a way to overcome monometal incomplete dehalogenation defects and an effective way to completely remove chlorinated contaminants [8]. In the last few decades, bimetal systems, including Pd/Fe, Ni/Fe, Ni/Si, Cu/Zn, and Cu/Fe, have significantly improved dechlorination [9]. Among these bimetal nanomaterials, the first metal is generally a metal with lower redox potential, such as Fe, Mg, Al, Zn, Sn, Si, etc., and is an electron donor, while the second metal is often a metal with high redox potential, such as Cu, Ni, Ag, and Pd. The second metal could be used as a hydrogenation catalyst to increase adsorption to hydrogen, thus improving the dechlorination efficiency of chlorinated organic matter. Among these metals, Fe and Pd are the most studied bimetallic materials because Fe is low in cost and Pd has good hydrogen storage activity. As a transition metal, Pd has vacant orbitals and can combine with substances containing π electrons with double bonds to form transition compounds, which reduce the bond energy of C-Cl, which is required for the reaction, thus speeding up the reaction rate [10]. The high price of Pd metal greatly limits its wide application. Therefore, cheap nickel metal is used to replace precious metals as a catalyst for the dechlorination of chlorinated organic matter. Therefore, Ni/Fe bimetallic nanomaterials are an effective approach to treating contaminated water containing chlorinated hydrocarbons. The synthesis of Ni/Fe has been demonstrated to achieve more radical dechlorination of halogenated organics by NaBH_4 co-reduction of Ni^{2+} and Fe^{2+} in an aqueous solution [11]. The use of Ni/Fe bimetal has many advantages. First, the metal Ni in the bimetal can be used as a catalyst, which effectively improves the hydrogenation dechlorination reaction. Second, metal Ni can also be used as an electron transfer medium, which can overcome the self-inhibition in electron transfer. Third, Ni/Fe nano-bimetal usually has a higher specific surface area and can have more active sites. The pH value of the system has a great influence on the performance of Fe. A low pH value ($\text{pH} < 4$) causes Fe to quickly disappear due to acidic corrosion ($2\text{Fe}^0 + 2\text{H}^+ \rightarrow \text{Fe}^{2+} + \text{H}_2$). High pH values ($\text{pH} > 10$) lead to iron precipitation through the formation of iron hydroxide and thus surface passivation ($\text{Fe}^0 + 2\text{H}_2\text{O} \rightarrow \text{Fe}^{2+} + \text{H}_2 + 2\text{OH}^-$). Both conditions are unfavorable to the hydrodechlorination of chlorinated hydrocarbons. Weak acid-base conditions ($4 < \text{pH} < 10$) are more favorable for rapid hydrodechlorination of chlorinated hydrocarbon pollutants in aqueous solution. The reaction processes occur as follows: $\text{RCl} + \text{Fe}^0 + \text{H}^+ \rightarrow \text{R-H} + \text{Fe}^{2+} + \text{Cl}^-$, $\text{Ni} + \text{H}_2 \rightarrow \text{Ni}\cdot\text{H}_2$, and $\text{Ni}\cdot\text{H}_2 + \text{Ni-R-Cl} \rightarrow \text{RH} + \text{H}^+ + \text{Cl}^- + 2\text{Ni}$. The dissolved oxygen (DO) value of the system has a great influence on the performance of Fe. DO and TCE decrease in synchronization and gradually decrease to a zero-oxygen state with the progress of the reaction. In terms of the reaction rates of hydrogen production and dechlorination, the reaction path of hydrodechlorination is also faster depending on the system's pH value [12]. Jian et al. reported the use of membrane-immobilized Ni-Fe for rapid transformation of TCE to ethane [13]. Schrick et al. showed that the dechlorination effect of synthetic Ni/Fe nano-bimetal was 280 times that of commercial iron powder, indicating that the dechlorination effect of nano-Ni/Fe was stronger than that of nano-iron [11].

This study aimed to synthesize Ni/Fe nano-bimetal by the NaBH_4 co-reduction method. TCE was selected as the target pollutant to explore the degradation efficiency and kinetics of Ni/Fe bimetallic particles on chlorinated hydrocarbons, determine the optimal load ratio, and analyze the degradation path and mechanism of the Ni-Fe bimetallic system on chlorinated hydrocarbons. The results provide a factual and theoretical basis for the subsequent application of nanoparticle metals in the environment. Previous reports show that an amorphous alloy structure can improve the reduction activity of a single metal [14]. The resulting Ni/Fe bimetallic nanomaterials as catalysts were analyzed by SEM, TEM, XRD, and XPS to evaluate the structure and the interaction between Ni and nZVIc. The effect of the mass ratio of Ni on the removal efficiency of TCE was also studied.

2. Material and Methods

2.1. Chemicals

Iron (III) chloride hexahydrate ($\text{FeCl}_3 \cdot 6\text{H}_2\text{O}$, AR $\geq 99.0\%$), Nickel (II) chloride hexahydrate ($\text{NiCl}_2 \cdot 6\text{H}_2\text{O}$, AR $\geq 99.0\%$), TCE (AR $\geq 99.5\%$), DCE (AR $\geq 99.5\%$), and NaBH_4 (AR $\geq 98.0\%$) were purchased from Greagent Reagent Co., Ltd. Methyl Alcohol (CH_3OH , HPLC $\geq 99.9\%$), Anhydrous ethanol ($\text{CH}_3\text{CH}_2\text{OH}$, HPLC $\geq 99.9\%$), hydrogen peroxide (H_2O_2 , AR $\geq 30\%$), 1-Bromo-4-Fluorobenzene (RG $\geq 98\%$), and hydrogen chloride (HCl, 36–38% | AR) were obtained from Adamas Reagent Co., Ltd. The deionized water (DW, resistivity $> 18.2 \text{ M}\Omega$, initial pH = 7.0 ± 0.1 , initial DO = 6.5 ± 0.1) used in this study was produced using the DirectPure UP HPLC $\geq 99.9\%$ system (Shanghai RephiLe Bioscience, Ltd., Shanghai, China).

2.2. Synthesis of Ni-nZVI Nanohybrids

Ni-nZVI was prepared by the NaBH_4 co-reduction method [15]. The specific steps were as follows: 150 mL deoxygenated DW and 350 mL deoxygenated ethanol were transferred into a three-necked flask and stirred at a fixed speed of 500 rpm. A solution of 18.23 mL of water containing 0.5 mol/L $\text{FeCl}_3 \cdot 6\text{H}_2\text{O}$ solution and certain amounts of 0.5 mol/L $\text{NiCl}_2 \cdot 6\text{H}_2\text{O}$ solution (0.091 mL, 0.136 mL, 0.915 mL, or 3.646 mL) was poured into a three-necked flask and stirred for another 20 min to achieve Ni/Fe proportions of 0.5%, 3%, 5% and 20 wt%. The 0.89 mol/L NaBH_4 (40 mL) solution was slowly added to the mixture and stirred for 30 min. During the preparation process, nitrogen was continuously injected. Ultimately, the black particles of Ni-nZVI that were obtained were washed with 400 mL of deoxy ethanol at least 6 times. The resulting black particles were stored in a 50 mL vial filled with deoxygenated ethanol until use.

2.3. Materials Characterization

X-ray diffraction (XRD) patterns were collected on a Rigaku Ultimate IV X-ray diffractometer with $\text{Cu-}\alpha$ radiation at 40 kV and 40 mA. Scanning electronic microscopy (SEM) images were recorded on a Hitachi S4800 spectrometer. The Brunauer–Emmett–Teller (BET) surface area was measured with a nitrogen adsorption instrument (Micromeritics ASAP 2460 analyzer) at liquid-nitrogen temperature. X-ray photoelectron spectrometer (XPS) surveys were carried out with a Xi photoelectron spectrometer with monochromatic $\text{Al-K}\alpha$ excitation ($h\nu = 1486.6 \text{ eV}$) to determine the chemical composition of the samples. The binding energy of the C 1s peak (284.8 eV) was used to calibrate the peak positions. The concentrations of chloride ions were determined by ion chromatography (Dionex ICS 6000, Thermo Fisher Scientific, California, CA, USA) using a hydrophilic anion-exchange column (Dionex IonPac™ AG11-HC (4 mm \times 250 mm)).

2.4. TCE Degradation

In accordance with the gravimetric method, TCE with a concentration of 400 $\mu\text{g/L}$ was prepared. According to the dosage of nZVI (1000 mg/L) required, a certain volume of Ni-Fe composite material ethanol solution was removed into a 40 mL brown reaction bottle at room temperature (26–28 °C). The Ni/Fe composite material was quickly sucked to the bottom of the bottle with magnets. After pouring out the supernatant, it was dried rapidly under nitrogen. After 40 mL of 400 $\mu\text{g/L}$ TCE solution was quickly added to the tubes, the degradation experiment ran for 5 h. Then, at each time point, two reaction samples were taken to detect DO and pH, and 5 mL of supernatant was absorbed with a sterilized syringe. After it was filtered through a filter membrane, this 5 mL was injected into the anion test tube, and the concentration of Cl^- was detected. After the remaining solution was passed through the 0.45 μm nylon filter membrane, the content of chlorinated hydrocarbon was measured by GC-MSD (Agilent Technologies 8890 GC system/5977B GC-MSD–Teledyne Tekmar purge and trap system). Test conditions were: mass spectrometry (MS); DB-VRX capillary chromatographic column (30 m long, thickness of 1.4 μm , diameter of 0.25 mm, USE, USA); high purity (99.999%) helium as a carrying gas; and starting temperature in the

GC oven set at 40 °C, maintained for 0.5 min, rising to 180 °C by a rate of 15.0 °C/min, then increasing at 15.0 °C/min to 200 °C, lasting 3.5 min. The ejector and detector temperatures were 220 °C and 250 °C, respectively. From the detected concentrations of TCE, pseudo-first-order rate constants were calculated with the equation: $\ln(C/C_0) = -K_{\text{obs}} t$, where K_{obs} = rate constant and C = the detected concentration of TCE at various stages (final, initial, and time-dependent). A plot of $\ln(C/C_0)$ against time was constructed for each kinetic run, and the initial slope was determined for the evaluation of the rate constant for each kinetic experiment with a fixed time method.

3. Results and Discussion

3.1. X-ray Diffractometry

As is shown in Figure 1, the diffraction peaks at 2θ (44.673° (110), 65.021° (200) and 82.333° (211)) were the characteristic diffraction peaks of Fe⁰ (PDF-#.06-0696) [16,17]. The composite material had only a wide peak near $2\theta = 44.673^\circ$, which indicates that Ni and Fe formed an amorphous alloy. Similar results were reported by Schrick et al. [18]. The bimetallic synergy caused by Ni addition might lead to a higher reduction activity, and this amorphous alloy structure is favorable for both reduction activities [14]. The diffraction peaks at 2θ equal to 44.507°, 51.846°, and 76.370° correspond to the (111), (200), and (220) planes of Ni metal (PDF-#.04-0850) [19,20]. Notably, 10% Ni-F material showed a Ni diffraction peak, probably because excess nickel covered the bimetallic surface [21]. It resulted in a failure to form a bimetallic system and the failure of pollutants to contact the zero-valent iron, reducing the degradation effect. Moreover, 10% and 0.5% Ni-nZVI composites exhibited a Fe₂O₃ diffraction peak at 8.68°, which might be due to the oxidation of partial Fe by O₂ in water during the synthesis [22].

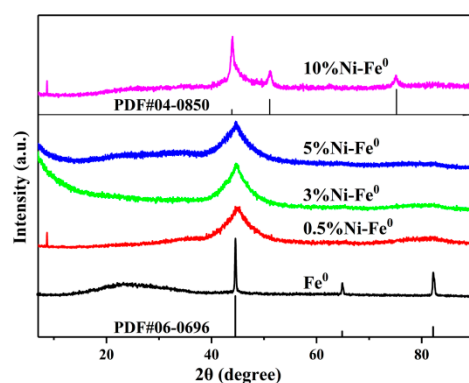


Figure 1. XRD images of nZVI and Ni-nZVI with different nickel contents.

3.2. Morphology

The monometallic nZVI and co-reduced bimetallic 5% Ni-nZVI were both approximately spherical or chain-like (the magnetic interaction between particles) with a size range of 20–50 nm (see SEM Figure 2a,b) [23,24]. There were no apparent size differences between monometallic nZVI and Ni-nZVI with different Ni mass ratios. This could be explained by the low molar concentrations of Ni²⁺ and Fe²⁺ and the use of excess NaBH₄ in the synthesis process, which resulted in uniformly distributed Ni-nZVI. Meanwhile, a uniform surface area was obtained by BET analysis (30–40 m²/g). Moreover, the uniform distribution of Ni-nZVI was observed from the EDS chart (see SEM-EDS Figure 2d–f), which might provide the basis for the synergistic action of bimetals, as reported by Nafis et al. [25]. Each particle consisted of a clear dark phase at its center, surrounded by a light layer corresponding to ZVI and a layer of passivated iron oxide (see TEM Figure 2c). However, the similarity of electron density between Ni and Fe made it impossible to determine the Ni doping position in nanoparticles from TEM.

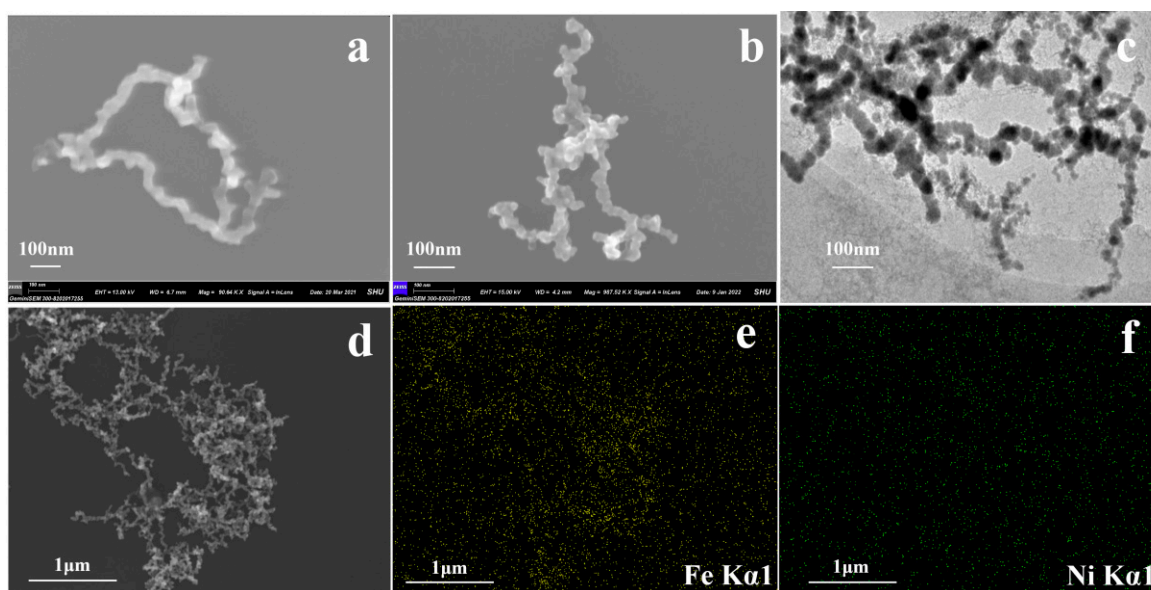


Figure 2. (a) SEM images of nZVI; (b) 5% Ni-nZVI; (c) TEM images of 5% Ni-nZVI; and (d–f) SEM-EDS of 5% Ni-nZVI.

3.3. X-ray Photoelectron Spectrometer

The elemental composition of the 5% Ni-nZVI composite along with its binding energy were analyzed by XPS (Figure 3). The oxygen spectrum deconvoluted into three types (Figure 3b): the anionic oxygen in the iron oxide of nZVI at about 529.60 eV; the oxygen-containing functional groups at about 531.18 eV; and the water at higher binding energies at 532.32 eV [26]. The chemical composition of nickel was identified by peak fitting, indicating that $\text{Ni}^{2+}/\text{Ni}^{3+}$ coexisted in the bimodal separation with binding energy at 856.48 eV ($\text{Ni } 2p_{3/2}$) and 874.09 eV ($\text{Ni } 2p_{1/2}$), and the binding energy difference was 17.61 eV. The result was the presence of $\text{Ni}(\text{OH})_2$ [27,28]. Ni doping increased the binding energy and promoted electron transfer, thus enhancing the reduction activity of the nickel-iron bimetallic material. According to Figure 3a, the signal peaks at 706.53 and 719.73 eV were attributable to the binding energy of Fe^0 . The signal peaks of Fe^{2+} (708.67, 717.99, 722.47, and 731.45 eV) and Fe^{3+} (711.26, 714.46, 724.65, and 727.26 eV) also appeared in the spectrum [29,30]. According to the peak area corresponding to each binding energy, the contents of Fe^0 , Fe^{2+} , and Fe^{3+} were 8.83%, 46.10%, and 45.07%, respectively, indicating that various forms of iron series were loaded on the surface of the Ni-nZVI composite. The results imply that part of the ZVI in the Ni-nZVI composite was oxidized into Fe^{2+} and Fe^{3+} during storage and characterization [31].

3.4. Morphology TCE Degradation by Ni-nZVI and nZVI

Figure 4 shows the degradation of TCE and DCE in the reaction system of Ni-nZVI with different nickel contents. The time for nZVI to completely degrade TCE was 5 h and 4 h for 0.5% Ni-nZVI, 2 h for 3% Ni-nZVI, 1 h for 5% Ni-nZVI, and 3 h for 10% Ni-nZVI. The bimetallic Ni-ZVI system degraded TCE 1.4–3.5 times faster than monometallic nZVI [11,32].

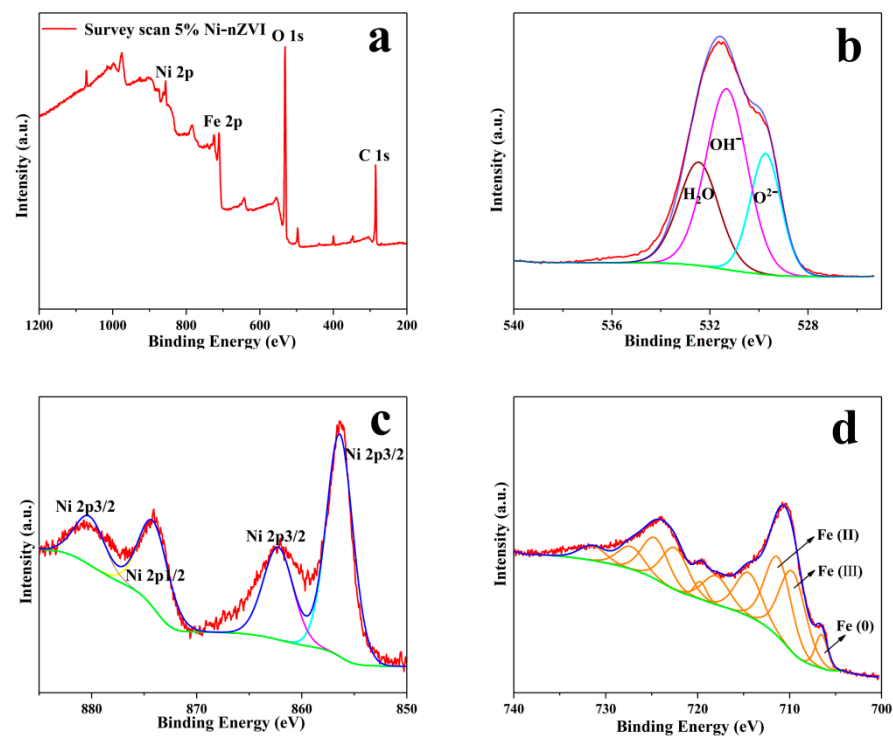


Figure 3. XPS analysis of 5% Ni-nZVI composite: (a) survey scans; (b) O1s; (c) Ni 2p; (d) Fe 2p.

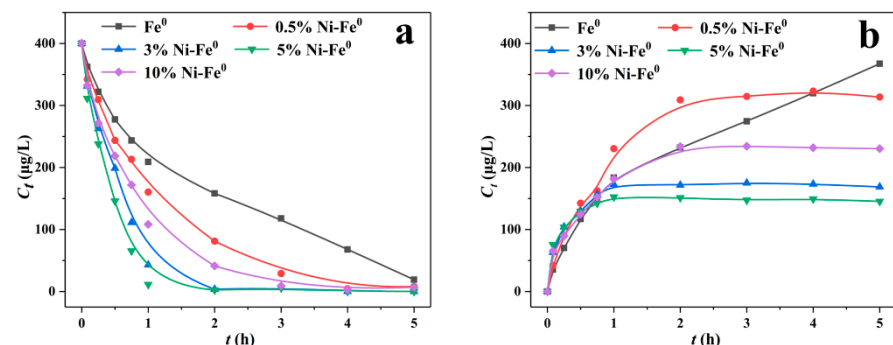


Figure 4. Degradation of TCE by Ni-nZVI with different nickel contents. Initial TCE concentration = 400 ± 10 $\mu\text{g/L}$; initial pH = 7.0 ± 0.1 , initial DO = 6.5 ± 0.1 ; nZVI for all experiments = 1000 mg/L; reaction volume = 40 mL. (a) TCE; (b) DCE.

Figure 5a–d show the change in chloride concentrations during the Ni-nZVI-degraded TCE reaction system. Total carbon with different Ni contents showed a decreasing trend in the Ni-nZVI reaction system. As ethylene and ethane were gaseous products at room temperature and pressure, GC-VRX could not detect them, so chlorine conservation was used for further analysis. The final dechlorination amount of the 0.5% Ni-nZVI composite was 21.62% of the initial amount, while that of the 3% Ni-nZVI composite was 57.82%, that of the 5% Ni-nZVI composite was 63.69%, and that of the 10% Ni-nZVI composite was 42.41%. Moreover, Ni-nZVI with 5 wt% of Ni contents had the best dechlorination effect: removal rates of TCE and its by-product DCE were 100% and 63.69%, respectively.

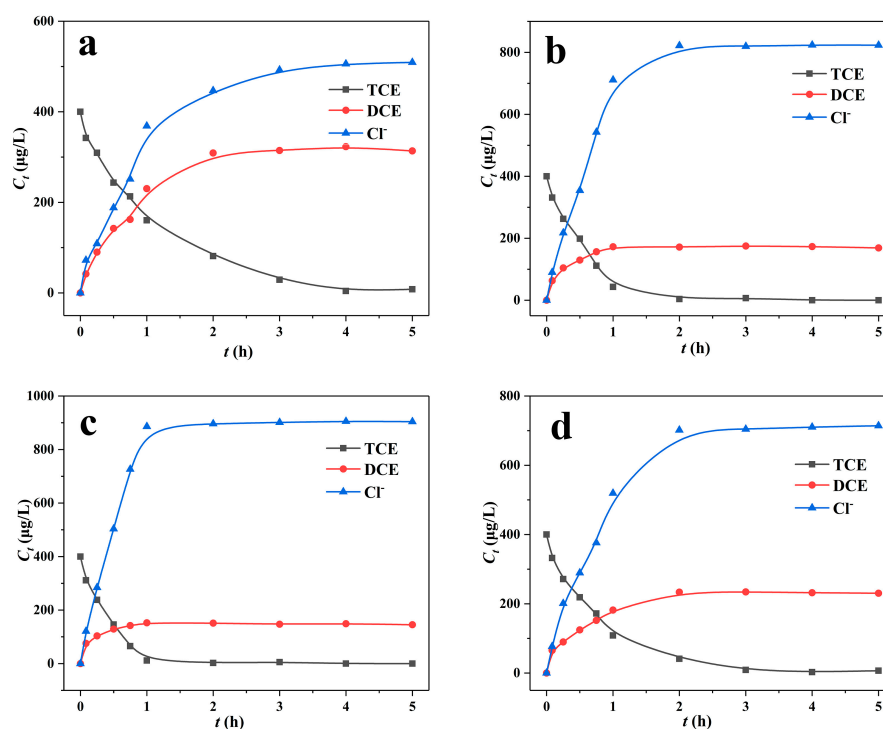


Figure 5. The concentrations of chloride ions for Ni-nZVI degradation with different Ni contents: (a) 0.5% Ni-nZVI; (b) 3% Ni-nZVI; (c) 5% Ni-nZVI; (d) 10% Ni-nZVI.

3.5. Kinetic Analysis of TCE Degradation with Different Ni Contents of Ni-nZVI

As shown in Table 1, the degradation reactions of ZVI in halogenated hydrocarbons were all fitted with pseudo-first-order reaction kinetics [33,34]. The value of K_{obs} in the kinetic equation represents the apparent degradation rate; the higher the value of K_{obs} , the higher the degradation efficiency. The degradation rate constant K of 5% Ni-nZVI was much higher than that of nZVI, which might be optimal due to Ni loading. The active sites on the bimetal surface provided a position for the reductive dechlorination of TCE. With increasing Ni content load, the degradation performance increased, and 5% Ni content achieved the optimal results. A Ni content of 10% reduced degradation due to excessive Ni load on the surface of nZVI, which prevented the release of nZVI and affected the contact between pollutants and ZVI at the same time.

Table 1. Kinetic parameters of TCE degradation.

The Reactants	Reaction Time (h)	Degradation Rate (%)	Correlation Coefficient	Reaction Rate K (h^{-1})
nZVI	1	47.85	0.98	0.675
0.5% Ni-nZVI	1	60.01	0.99	0.909
3% Ni-nZVI	1	89.28	0.99	1.663
5% Ni-nZVI	1	98.18	0.99	2.358
10% Ni-nZVI	1	72.91	0.99	1.250

3.6. pH DO Change Analysis

The changes in pH and DO during the degradation of TCE in the bimetallic system are shown in Figure 6a,b, respectively. With the progress of the reaction, DO and TCE decreased in synchronization and gradually decreased to a zero-oxygen state. Meanwhile, pH gradually increased from 7 to about 8.8. The results show that pH and DO in solution were closely related to the degradation of TCE. The effect of pH on the reaction might be attributed to the participation of protons in the dechlorination reaction [35,36].

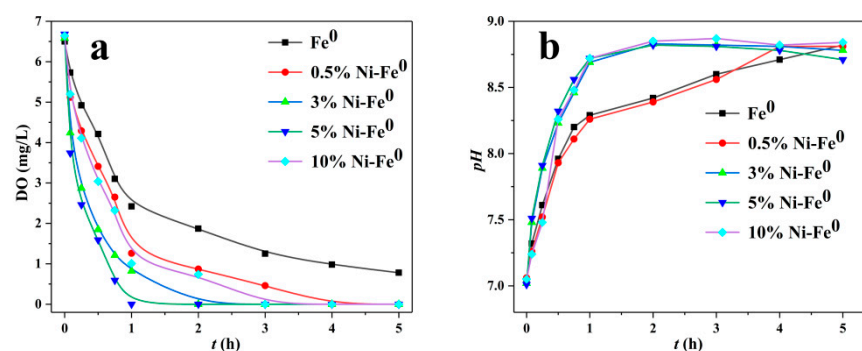


Figure 6. Changes in pH and DO during the degradation of TCE by Ni-nZVI with different nickel contents: (a) DO; (b) pH.

4. Conclusions

In this study, the reactivity of Ni/Fe nanoparticles and monometallic nZVI to TCE dechlorination has been systematically studied. Ni/Fe composites were prepared by the NaBH_4 co-reduction method, which was characterized by XRD, SEM, BET, and XPS. SEM and XRD results showed that the Ni/Fe nanoparticles were successfully formed into amorphous alloys, and the Ni/Fe distribution was uniform. This amorphous alloy structure could improve the reduction activity of a single metal. By analyzing TCE degradation, it was found that the degradation efficiency of zero-valent iron particles was greatly improved, and the degree of dechlorination was more thorough after bimetallic modification. The apparent rates of TCE with Ni-Fe all appeared to be quantified with a pseudo-first-order kinetic model. The degradation efficiency first increased and then decreased with the increase in Ni. When Ni content was 5%, the maximum degradation kinetic constant was 2.358 h^{-1} . The highest degradation rate of the Ni/Fe catalytic system was four times higher than that of a general single metal catalyst, which certified its efficient catalytic reduction capability. Ni metal is cheap and plentiful. Therefore, Ni/Fe composites have a great potential to be used as suitable materials for the remediation of halogenated organic compounds in polluted sites or plant treatment. In such cases, they could be applied as prospective materials for permeable reactive barriers or be used for high-end applications, e.g., the advanced treatment of groundwater or surface water.

Author Contributions: X.L.: Writing—original draft, Investigation, Data curation; J.Z.: Data curation, Writing—review and editing; M.W.: Supervision, Resources, Funding acquisition. All authors have read and agreed to the published version of the manuscript.

Funding: This work was supported by the Guangdong Basic and Applied Basic Research Foundation (2020A1515110591).

Institutional Review Board Statement: Not applicable.

Informed Consent Statement: Informed consent was obtained from all subjects involved in the study.

Data Availability Statement: Not applicable.

Conflicts of Interest: On behalf of all authors, the corresponding author states that there is no conflict of interest.

References

1. Karn, B.; Kuiken, T.; Otto, M. Nanotechnology and in situ remediation: A review of the benefits and potential risks. *Environ. Health Perspect.* **2009**, *117*, 1823–1831. [[CrossRef](#)] [[PubMed](#)]
2. Freirla-Gádara, M.J.; Lorenzo-Perreira, R.A.; Alvarez-Devesa, A.; Bermejo, F. Occurrence of halogenated hydrocarbons in the water supply of different cities of alicia (Spain). *Environ. Technol.* **1992**, *13*, 437–447. [[CrossRef](#)]
3. Wang, S.; Deng, Y.; Shao, B. Reinvestigation of the oxidation of organic contaminants by Fe(VI): Kinetics and effects of water matrix constituents. *J. Hazard. Mat.* **2022**, *430*, 128421. [[CrossRef](#)] [[PubMed](#)]
4. Sohn, K.; Kang, S.W.; Ahn, S.; Woo, M.; Yang, S.K. Fe (0) nanoparticles for nitrate reduction: Stability, reactivity, and transformation. *Environ. Sci. Technol.* **2006**, *40*, 5514–5519. [[CrossRef](#)] [[PubMed](#)]

5. Kim, H.-S.; Kim, T.; Ahn, J.-Y.; Hwang, K.-Y.; Park, J.-Y.; Lim, T.-T. Aging characteristics and reactivity of two types of nanoscale zero-valent iron particles (Fe⁰BH and Fe⁰H₂) in nitrate reduction. *Chem. Eng. J.* **2012**, *197*, 16–23. [[CrossRef](#)]
6. Chi, H.N.; Mai, L.T.; Tran, T.; Juang, R.S. Efficient removal of antibiotic oxytetracycline from water by Fenton-like reactions using reduced graphene oxide-supported bimetallic Pd/nZVI nanocomposites. *J. Taiwan Inst. Chem. E.* **2021**, *119*, 80–89.
7. Yu, Y.; Zheng, H.; Deng, D.; Ju, Y.; Hui, L. Synthesis of millimeter-scale sponge Fe/Cu bimetallic particles removing TBBPA and insights of degradation mechanism. *Chem. Eng. J.* **2017**, *325*, 279–288. [[CrossRef](#)]
8. Liu, Y.; Yang, F.; Yue, P.L.; Chen, G. Catalytic dechlorination of chlorophenols in water by palladium/iron. *Water Res.* **2001**, *35*, 1887–1890. [[CrossRef](#)]
9. Fennelly, J.P.; Roberts, A.L. Reaction of 1,1,1-trichloroethane with zero-valent metals and bimetallic reductants. *Environ. Sci. Technol.* **1998**, *32*, 1980–1988. [[CrossRef](#)]
10. Elliott, D.W.; Zhang, W.X. Field assessment of nanoscale bimetallic particles for groundwater treatment. *Environ. Sci. Technol.* **2001**, *35*, 4922–4926. [[CrossRef](#)]
11. Schrick, B.; Blough, J.L.; Jones, Daniel, A.; Mallouk, T.E. Hydrodechlorination of trichloroethylene to hydrocarbons using bimetallic Nickel-Iron nanoparticles. *Chem Mater.* **2002**, *14*, 5140–5147. [[CrossRef](#)]
12. Li, C.J.C.; Rao, P.; Annable, M. Degradation of perchloroethylene in cosolvent solutions by zero-valent iron. *J. Hazard. Mater.* **2003**, *96*, 65–78.
13. Jian, X.; Dozier, A.; Bhattacharyya, D. Synthesis of nanoscale bimetallic particles in polyelectrolyte membrane matrix for reductive transformation of halogenated organic compounds. *J. Nanopart. Res.* **2005**, *7*, 449–467.
14. Yamashita, H.; Yoshikawa, M.; Funabiki, T.; Yoshida, S. Catalysis by amorphous metal alloys. *J. Catal.* **1986**, *99*, 375–382. [[CrossRef](#)]
15. Wang, C.B.; Zhang, W.X. Synthesizing nanoscale iron particles for rapid and complete dechlorination of TCE and PCBs. *Environ. Sci. Technol.* **1997**, *31*, 9602–9607. [[CrossRef](#)]
16. Dong, H.; Deng, J.; Xie, Y.; Zhang, C.; Jiang, Z.; Cheng, Y. Stabilization of nanoscale zero-valent iron (nZVI) with modified biochar for Cr (VI) removal from aqueous solution. *J. Hazard. Mater.* **2017**, *332*, 79–86. [[CrossRef](#)]
17. Fan, M.; Li, T.; Hu, J.; Cao, R.; Wu, Q.; Wei, X. Synthesis and characterization of reduced graphene oxide-supported nanoscale zero-valent iron (nZVI/rGO) composites used for Pb (II) removal. *Materials* **2016**, *9*, 687. [[CrossRef](#)]
18. Li, F.; Vipulanandan, C. Microemulsion and solution approaches to nanoparticle iron production for degradation of trichloroethylene. *Colloids Surf. A Physicochem. Eng. Asp.* **2013**, *223*, 103–112. [[CrossRef](#)]
19. Pandey, D.; Ray, K.; Bhardwaj, R.; Bojja, S.; Chary KV, R.; Deo, G. Promotion of unsupported nickel catalyst using iron for CO₂ methanation. *Int. J. Hydrog. Energy.* **2018**, *43*, 4987–5000. [[CrossRef](#)]
20. Pandey, D.; Deo, G. Effect of support on the catalytic activity of supported Ni–Fe catalysts for the CO₂ methanation reaction. *J. Ind. Eng. Chem.* **2016**, *33*, 99–107. [[CrossRef](#)]
21. Wu, L.; Ritchie, S.M. Removal of trichloroethylene from water by cellulose acetate supported bimetallic Ni/Fe nanoparticles. *Chemosphere* **2006**, *63*, 285–292. [[CrossRef](#)] [[PubMed](#)]
22. Wang, S.; Zhou, Y.; Gao, B.; Wang, X.; Yin, X.; Feng, K. The sorptive and reductive capacities of biochar supported nanoscaled zero-valent iron (nZVI) in relation to its crystallite size. *Chemosphere* **2017**, *186*, 495–500. [[CrossRef](#)] [[PubMed](#)]
23. Busch, J.; Meißner, T.; Potthoff, A.; Bleyl, S.; Georgi, A.; Mackenzie, K.; Trabitzsch, R.; Werban, U.; Oswald, S.E. A field investigation on transport of carbon-supported nanoscale zero-valent iron (nZVI) in groundwater. *J. Hydrol.* **2015**, *181*, 59–68. [[CrossRef](#)] [[PubMed](#)]
24. Li, X.; Zeng, L.; Wen, N.; Deng, D. Critical roles of sulfidation solvent in controlling surface properties and the dechlorination reactivity of S-nZVI. *J. Hazard. Mater.* **2021**, *417*, 126014. [[CrossRef](#)]
25. Gangopadhyay, S.; Hadjipanayis, G.C.; Sorensen, C.M.; Klabunde, K.J. Exchange anisotropy in oxide passivated Co fine particles. *J. Appl. Phys.* **1993**, *73*, 6964–6966. [[CrossRef](#)]
26. Yao, Y.H.; Huang, S.M.; Zhou, W. Highly dispersed core-shell iron nanoparticles decorating onto graphene nanosheets for superior Zn (II) wastewater treatment. *Environ. Sci. Pollut. Res.* **2018**, *26*, 806–815. [[CrossRef](#)]
27. Ji, S.T.; Giang, B.L.; Sharanjit, S.; Duc, T.Q.; Thanh, H.; Huu, H. Methane bi-reforming over boron-doped Ni/SBA-15 catalyst: Longevity evaluation. *Int. J. Hydrog. Energy.* **2018**, *44*, 20839–20850.
28. Wang, Z.; Dong, P.; Sun, Z.; Sun, C.; Bu, H.Y.; Han, J. NH₂-Ni-MOF electrocatalysts with tunable size/morphology for ultrasensitive C-reactive protein detection via an aptamer binding induced DNA walker—Antibody sandwich assay. *J. Mater. Chem B.* **2018**, *6*, 2426–2431. [[CrossRef](#)]
29. Tao, L.; Ai, Z.; Zhang, L. Fe@Fe₂O₃ core—Shell nanowires as iron reagent. 4. Sono—Fenton degradation of pentachlorophenol and the mechanism analysis. *J. Phys. Chem. C.* **2008**, *112*, 8675–8681.
30. Antony, J.; Meera, V.; Raphael, V.P. Investigations on the capacity and mechanism of iron uptake by nano zero-valent iron particles. *B Mater. Sci.* **2021**, *44*, 1–11. [[CrossRef](#)]
31. Xiao, Y.; Liu, X.; Huang, Y.; Kang, W.; Wang, Z.; Zheng, H. Roles of hydroxyl and carbonate radicals in bisphenol a degradation via a nanoscale zero-valent iron/percarbonate system: Influencing factors and mechanisms. *RSC Adv.* **2021**, *11*, 3636–3644. [[CrossRef](#)] [[PubMed](#)]
32. Bokare, A.D.; Chikate, R.C.; Rode, C.V.; Paknikar, K.M. Iron-nickel bimetallic nanoparticles for reductive degradation of azo dye Orange G in aqueous solution. *Appl. Catal. B* **2008**, *79*, 270–278. [[CrossRef](#)]

33. Zhu, X.; Zhou, L.; Li, Y.; Han, B.; Feng, Q. Rapid degradation of carbon tetrachloride by microscale Ag/Fe bimetallic particles. *Int. J. Environ. Res. Public Health* **2021**, *18*, 2124. [[CrossRef](#)] [[PubMed](#)]
34. Liu, T.; Zhang, Z.; Wang, Z.; Wang, Z.L.; Bush, R. Highly efficient and rapid removal of arsenic (III) from aqueous solutions by nanoscale zero-valent iron supported on a zirconium 1,4-dicarboxybenzene metal—Organic framework (UiO-66 MOF). *RSC Adv.* **2019**, *9*, 39475–39487. [[CrossRef](#)]
35. Zhang, S.S.; Yang, N.; Zhuang, X.; Ren, L.; Zhan, J. Montmorillonite immobilized Fe/Ni bimetallic prepared by dry in-situ hydrogen reduction for the degradation of 4-Chlorophenol. *Sci. Rep.* **2019**, *9*, 1–9. [[CrossRef](#)]
36. Ying, G.A.; Fw, A.; Yan, W.A.; Ren, B.; Zca, B. Comparison of degradation mechanisms of microcystin-LR using nanoscale zero-valent iron (nZVI) and bimetallic Fe/Ni and Fe/Pd nanoparticles. *Chem. Eng. J.* **2016**, *285*, 459–466.